catalysts

MDPI

Article

Defective TiO_2 Core-Shell Magnetic Photocatalyst Modified with Plasmonic Nanoparticles for Visible Light-Induced Photocatalytic Activity

Zuzanna Bielan [1,*], Agnieszka Sulowska [1], Szymon Dudziak [1], Katarzyna Siuzdak [2], Jacek Ryl [3] and Anna Zielińska-Jurek [1,*]

1 Department of Process Engineering and Chemical Technology, Faculty of Chemistry, Gdansk University of Technology (GUT), G. Narutowicza 11/12, 80-233 Gdansk, Poland; Sulowska.as@gmail.com (A.S.); dudziakszy@gmail.com (S.D.)

2 Physical Aspects of Ecoenergy Department, The Szewalski Institute of Fluid-Flow Machinery Polish Academy of Science, Fiszera 14, 80-231 Gdansk, Poland; katarzyna.siuzdak@imp.gda.pl

3 Department of Electrochemistry, Corrosion and Materials Engineering, Faculty of Chemistry, Gdansk University of Technology (GUT), G. Narutowicza 11/12, 80-233 Gdansk, Poland; jacek.ryl@pg.edu.pl

* Correspondence: zuzanna.bielan@gmail.com (Z.B.); annjurek@pg.edu.pl (A.Z.-J.)

Received: 19 May 2020; Accepted: 11 June 2020; Published: 15 June 2020

Abstract: In the presented work, for the first time, the metal-modified defective titanium(IV) oxide nanoparticles with well-defined titanium vacancies, was successfully obtained. Introducing platinum and copper nanoparticles (NPs) as surface modifiers of defective d-TiO_2 significantly increased the photocatalytic activity in both UV-Vis and Vis light ranges. Moreover, metal NPs deposition on the magnetic core allowed for the effective separation and reuse of the nanometer-sized photocatalyst from the suspension after the treatment process. The obtained Fe_3O_4@SiO_2/d-TiO_2-Pt/Cu photocatalysts were characterized by X-ray diffractometry (XRD) and specific surface area (BET) measurements, UV-Vis diffuse reflectance spectroscopy (DR-UV/Vis), X-ray photoelectron spectroscopy (XPS) and transmission electron microscopy (TEM). Further, the mechanism of phenol degradation and the role of four oxidative species (h^+, e^-, $^\bullet OH$, and $^\bullet O_2^-$) in the studied photocatalytic process were investigated.

Keywords: titanium vacancies; phenol degradation; scavengers; magnetic photocatalysts; platinum-modified defective TiO_2

1. Introduction

In recent years, among wastewater treatment and environmental remediation technologies, photocatalysis has gained attention as a promising technique for the degradation of persistent organic pollutants at ambient temperature and pressure [1–4]. Pilot scale-installations for water treatment using photocatalysis are more and more popular among the world [5,6]. The structural and surface properties of photocatalysts significantly influence their physicochemical and photocatalytic properties. In this regard, one of the most important issues in the photocatalytic process is the preparation of well-characterized and highly active photocatalytic material.

Titanium(IV) oxide (TiO_2), the most widely used semiconductor in photocatalysis, is extensively exploited to obtain highly photoactive in UV-Vis range semiconductor material. The TiO_2 nanoparticles differing in size and surface area. Nonetheless, despite different morphology and polymorphic composition, all pristine titanium(IV) oxide particles own wide bandgap energy (Eg), which differs in the range of 3.0–3.2 eV, for rutile and anatase, respectively [7]. In this regard, TiO_2 photoexcitation is possible only with UV irradiation ($\lambda < 388$ nm), and therefore the application of solar radiation is highly limited.

Much effort has been done to shift TiO_2 excitation energy to longer wavelengths, especially in visible light range (400–750 nm). Among various methods [8–10], surface modification with noble and semi-noble metals is the most widely used and effective method. Wysocka et al. [11] obtained mono- (Pt, Ag, and Cu) and bimetal- (Cu/Ag, Ag/Pt, and Cu/Pt) modified TiO_2 photocatalysts, where TiO_2 matrix was commercially available ST01 (fine anatase particles). Metal ions were reduced using the chemical ($NaBH_4$ solution) as well as thermal treatment methods. Klein et al. [12] prepared TiO_2-P25 modified with Pt, Pd, Ag, and Au using radiolysis reduction. Obtained photocatalysts were further immobilized on the glass plate and used for toluene removal from the gas phase. Moreover, Janczarek et al. [13] proposed a method of obtaining Ag- and Cu-modified decahedral anatase particles (DAP) by photodeposition. Wei et al. [14] reported that selective deposition of nanometals (Au/Ag nanoarticles) on (001) facets of decahedral anatase particles (DAP), together with octahedral anatase particles (OAP) result in significant photocatalytic process improvement under visible light irradiation.

Another possibility of titania visible light activation is the introduction of intrinsic defects to its crystal structure. Titanium or oxygen vacancies and surface disorders led to changes in electronic and crystal changes, resulting in better electrons and holes separation and even bandgap narrowing [15]. Defected TiO_2 is often evidenced by their color: pale blue for oxygen vacancies (due to d–d transitions of bandgap states) and yellow for titanium vacancies (consumption of free electrons and holes), which also suggest shifting its light absorption to the visible light range [15].

Nevertheless, TiO_2 particle size and shape determine not only the number of active sites but also separation and reusability properties. Commercially available titanium(IV) oxide—P25 forms a stable suspension due to its nanometric sizes, which cause the detached process to be highly expensive and energy-consuming [16,17]. The immobilization of nanoparticles on solid substrates [18] could, in turn, result in a decrease in photocatalytic activity due to significantly reducing specific surface area [19,20]. Alternative way of photocatalyst separation is its deposition on magnetic compound, such as Fe_3O_4 [21,22], $CoFe_2O_4$ [23], $ZnFe_2O_4$ [24], and $BaFe_{12}O_{19}$ [25]. Along with using magnetic materials, the percentage of photocatalyst recovery and the possibility of its reuse significantly increase [26–29]. However, the direct contact of ferrite particles with photocatalyst (e.g., TiO_2) may result in unfavorable electron transfer from TiO_2 into the magnetic compound, causing its transformation and photocorrosion [26]. Thus, their separation with an inert interlayer of silica [26–31] or carbon [32] could effectively prevent the charge carriers recombination. In this regard, the magnetic Fe_3O_4@SiO_2/TiO_2 nanocomposites with a core-shell structure, where the core was Fe_3O_4, the photoactive shell was TiO_2, and silica was used as an inert interlayer, are a relatively new and promising group of composite materials.

The previous studies focused on the preparation and characterization of noble metal NPs modified with different titania matrices [33,34], as well as TiO_2 nanoparticles deposited on various magnetic cores (Fe_3O_4, $CoFe_2O_3$, and $ZnFe_2O_4$) [26–29]. However, in the literature, there is a lack of complex researches on the correlation between structural defects and TiO_2 modification with different materials (metal nanoparticles or other oxides).

In this regard, deeply characterized defective d-TiO_2 with stable titanium vacancies, obtained by a simple hydrothermal method was further modified with Pt and Cu nanoparticles as well as deposited on the magnetite core. The obtained samples were characterized by X-ray diffractometry (XRD), specific surface area (BET) measurements, UV-Vis diffuse reflectance spectroscopy (DR-UV/Vis), X-ray photoelectron spectroscopy (XPS), and transmission electron microscopy (TEM). The photodegradation of phenol as a model organic pollutant in the presence of the obtained photocatalysts was subsequently investigated in the range of UV-Vis and Vis irradiation. Further, the mechanism of phenol degradation and the role of four oxidative species (h^+, e^-, $^\bullet OH$, and $^\bullet O_2^-$) in the studied photocatalytic process were investigated.

MOST WIEDZY Downloaded from mostwiedzy.pl

2. Results

2.1. Physicochemical Characterization of d-TiO_2-Pt/Cu and Magnetic Fe_3O_4@SiO_2/d-TiO_2-Pt/Cu Photocatalysts

The preparation of d-TiO_2 photocatalysts was based on the hydrothermal method in the oxidative environment (addition of 20–75 mol% of HIO_3). The electron paramagnetic resonance (EPR) analysis confirmed the presence of titanium vacancies with g value of 1.995 after calcination. The signal at EPR spectra for bulk Ti^{3+} was not observed for pure TiO_2 sample, see in Figure 1.

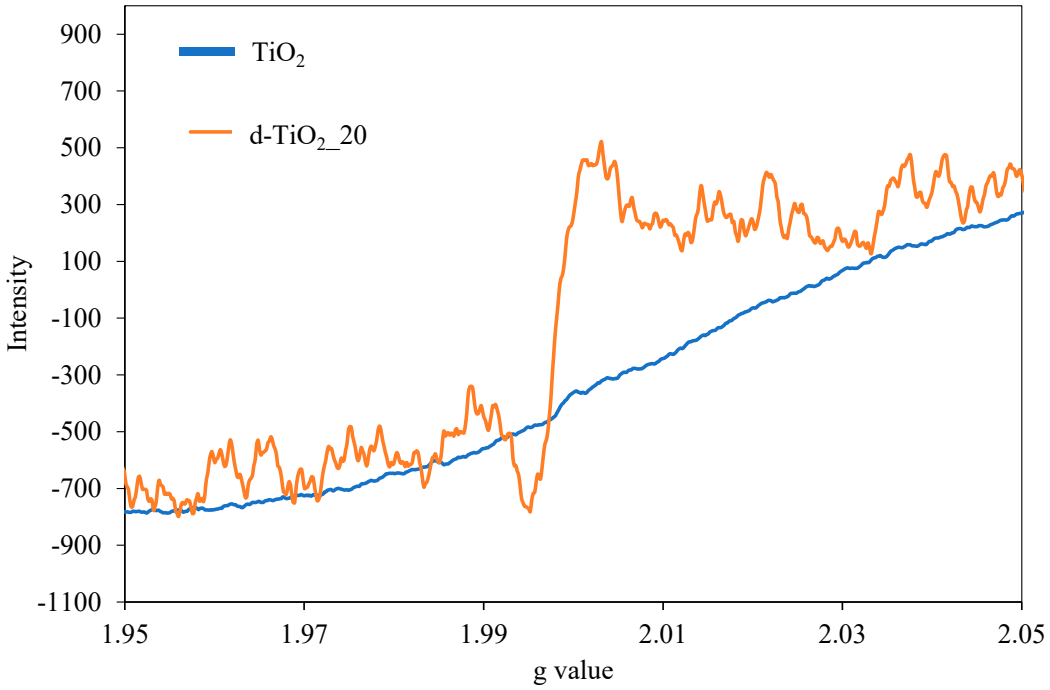

Figure 1. The electron paramagnetic resonance (EPR) spectra in the room temperature for TiO_2 (blue line) and TiO_2 with titania vacancies (orange line).

The general physicochemical and photocatalytic characteristics of the obtained defective d-TiO_2-Pt/Cu and Fe_3O_4@SiO_2/d-TiO_2-Pt/Cu samples, i.e., BET surface area, pore volume, calculated bandgap (Eg) and phenol degradation efficiency in UV-Vis and Vis light are presented in Tables 1 and 2.

MOST WIEDZY Downloaded from mostwiedzy.pl

Table 1. Physicochemical and photocatalytic characteristics of the obtained defective d-TiO_2-Pt/Cu samples.

Sample	BET ($m^2 \cdot g^{-1}$)	V Pores ($cm^3 \cdot g^{-1}$)	Eg (eV)	Rate Constant k (min^{-1})·10^{-2} UV-Vis	Phenol Removal (%) UV-Vis	Rate Constant k (min^{-1})·10^{-2} Vis	Phenol Removal (%) Vis
TiO_2	169	0.0836	3.2	0.98	46	0.03	3
d-TiO_2_20	172	0.0847	2.7	0.79	40	0.17	13
d-TiO_2_75	167	0.0826	2.9	0.52	29	0.03	4
TiO_2-Pt0.05	166	0.0819	3.2	2.30	76	0.22	14
d-TiO_2_20-Pt0.05	148	0.0727	2.85	1.10	48	0.33	20
d-TiO_2_75-Pt0.05	164	0.0808	2.9	1.02	46	0.26	15
d-TiO_2_20-Pt0.1	152	0.0747	2.7	1.42	57	0.41	22
d-TiO_2_20-Cu0.1	101	0.0499	2.9	0.51	30	0.12	7
d-TiO_2_20-Pt0.1/Cu0.1	152	0.0744	2.75	1.47	59	0.27	17

Table 2. Physicochemical and photocatalytic characteristics of the obtained magnetic Fe_3O_4@SiO_2/d-TiO_2-Pt/Cu samples.

Sample	BET ($m^2 \cdot g^{-1}$)	V Pores ($cm^3 \cdot g^{-1}$)	Rate Constant k (min^{-1})·10^{-2} UV-Vis	Phenol Removal (%) UV-Vis	Rate Constant k (min^{-1})·10^{-2} Vis	Phenol Removal (%) Vis
Fe_3O_4@SiO_2/d-TiO_2_20	117	0.0578	0.41	20	0.13	8
Fe_3O_4@SiO_2/d-TiO_2_20-Pt0.05	115	0.0568	0.15	11	0.08	4
Fe_3O_4@SiO_2/d-TiO_2_20-Pt0.1	122	0.0602	0.41	19	0.19	11
Fe_3O_4@SiO_2/d-TiO_2_20-Cu0.1	117	0.0579	0.22	15	0.05	2
Fe_3O_4@SiO_2/d-TiO_2_20-Pt0.1/Cu0.1	117	0.0580	0.36	22	0.26	11

MOST WIEDZY Downloaded from mostwiedzy.pl

The BET surface area of pure TiO_2 obtained from Titanium(IV) butoxide (TBT) hydrolysis in water and defective TiO_2 samples was similar and ranged from 167 to 172 $m^2 \cdot g^{-1}$. The specific surface area of the metal-modified d-TiO_2 samples fluctuated from 166 to 101 $m^2 \cdot g^{-1}$ and depended on the type and amount of metallic species deposited on d-TiO_2 surface. The samples modified with Pt NPs revealed a higher BET surface area of about 148 $m^2 \cdot g^{-1}$ compared to d-TiO_2 modified with copper oxide (101 $m^2 \cdot g^{-1}$), and bimetallic Pt/Cu NPs (152 $m^2 \cdot g^{-1}$). The relations between photoactivity in UV-Vis and Vis light range versus BET surface area are also shown in Tables 1 and 2. The obtained results indicated that not so much the surface area but rather the presence of Ti defects and modification with metal nanoparticles caused the enhanced photoactivity of the obtained photocatalysts. Moreover, as shown in Table 2, the addition of surface-modifying metal nanoparticles, as well as further deposition of d-TiO_2-Pt/Cu on magnetic matrice, did not affect the magnitude order of the BET surface area, which remained in the range of 101 to 172 $m^2 \cdot g^{-1}$ for d-TiO_2_20-Cu0.1 and d-TiO_2_20, respectively.

The energy bandgaps for all samples were calculated from the plot of (Kubelka–Munk·E)$^{0.5}$ versus E, where E is energy equal to hv, and summarized in Table 1. The samples consist of defective TiO_2 exhibited narrower bandgap of 2.7–2.9 eV compared to TiO_2 and TiO_2-Pt0.05 photocatalysts. Moreover, for all metal-modified defective photocatalysts, the bandgap value, calculated from Kubelka–Munk, transformation did not change, compared to d-TiO_2 matrice, indicating surface modification than doping [11].

The XRD patterns for selected d-TiO_2-Pt/Cu and Fe_3O_4@SiO_2/d-TiO_2-Pt/Cu samples are presented in Figures 1 and 2, with a detailed phase composition and crystalline sizes for all photocatalysts being listed in Tables 3 and 4. Peaks marked "A", "R", and "B" corresponds to anatase, rutile, and brookite phases, respectively. Both crystalline structures (anatase and brookite) appeared for pure TiO_2 prepared by the sol–gel method. For Pt-modified TiO_2 anatase was the major phase, whereas brookite existed as the minor phase. The average crystallite size of anatase was 5–6 nm. The preparation of d-TiO_2 photocatalysts proceeded in the oxidative environment. The introduction into the crystal structure of various types of defects promotes the transformation of anatase to rutile at lower temperatures. Therefore, for the samples obtained in the presence of HIO_3 as the oxidizing agent, after the annealing process the percentage of anatase (the most intense peak at 25° 2θ, with the (101) plane diffraction, ICDD's card No. 7206075) was decreased in favor of (110) rutile, with the peak at 31° 2θ (ICDD's card No. 9004141), even below the anatase to rutile phase transformation temperature [35–37]. For the samples d-TiO_2_75 and d-TiO_2_75-Pt0.05, the dominant phase was rutile with a crystallite size of about 6 nm. Further, the surface modification with plasmonic platinum and semi-noble copper did not cause changes in anatase crystallite size, remaining about 5–6 nm size. The percentage of the brookite phase increased to 8.5% and 13% for d-TiO_2 _20-Pt0.1/Cu0.1, and d-TiO_2_20-Pt0.1 samples, respectively. It resulted from the additional thermal treatment after metal nanoparticles deposition on the photocatalyst surface. Moreover, Pt and Cu modification of TiO_2 did not cause the shift of the peaks in the XRD pattern. The presence of platinum and copper deposited on TiO_2 was not approved (no peaks for platinum or copper) due to low content (0.05–0.1 mol%) and nanometric size.

MOST WIEDZY Downloaded from mostwiedzy.pl

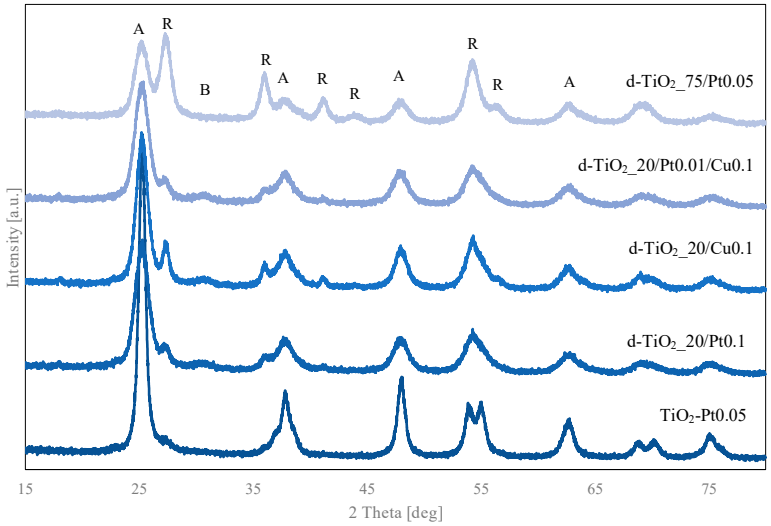

Figure 2. X-ray diffractometry (XRD) patterns for selected defective d-TiO_2-Pt/Cu photocatalysts (A—anatase, B—brookite, and R—rutile).

MOST WIEDZY Downloaded from mostwiedzy.pl

Table 3. Crystalline phases characteristic for obtained defective d-TiO_2-Pt/Cu samples.

Sample	Crystalline Size and Phase Content					
	Anatase		Rutile		Brookite	
	Size (nm)	Phase Content (wt.%)	Size (nm)	Phase Content (wt.%)	Size (nm)	Phase Content (wt.%)
TiO_2	5.97 ± 0.04	95.5 ± 1	-	-	6.1 ± 0.3	4.5 ± 1
d-TiO_2_20	5.14 ± 0.03	96 ± 1.0	-	-	4.0 ± 0.6	3.5 ± 0.5
d-TiO_2_75	5.67 ± 0.05	21 ± 3.5	6.57 ± 0.09	80 ± 2	-	-
TiO_2-Pt0.05	5.71 ± 0.06	91 ± 0.5	-	-	5.7 ± 0.6	9 ± 1
d-TiO_2_20-Pt0.05	5.66 ± 0.03	85 ± 8	9.8 ± 0.7	9 ± 1.0	4.9 ± 0.3	6 ± 0.5
d-TiO_2_75-Pt0.05	5.49 ± 0.04	48 ± 2	7.53 ± 0.12	52 ± 2	-	-
d-TiO_2_20-Pt0.1	5.58 ± 0.03	81 ± 8	7.6 ± 0.8	6 ± 1	4.8 ± 0.3	13 ± 1
d-TiO_2_20-Cu0.1	6.62 ± 0.04	72 ± 11	11.7 ± 0.4	9 ± 2	1.52 ± 0.08	8.5 ± 1
d-TiO_2_20-Pt0.1/Cu0.1	5.52 ± 0.03	83 ± 12	9.5 ± 0.6	8 ± 2	5.1 ± 0.3	8.5 ± 1

Table 4. Crystalline phases characteristic for the obtained magnetic Fe_3O_4@SiO_2/d-TiO_2_20-Pt/Cu samples.

Sample	Crystalline Size and Phase Content					
	Anatase		Rutile		Magnetite	
	Size (nm)	Phase Content (wt.%)	Size (nm)	Phase Content (wt.%)	Size (nm)	Phase Content (wt.%)
Fe_3O_4@SiO_2/d-TiO_2_20	5.19 ± 0.05	71 ± 1.5	8.6 ± 0.5	8 ± 0.5	46.1 ± 1.1	21 ± 0.5
Fe_3O_4@SiO_2/d-TiO_2_20-Pt0.05	5.60 ± 0.05	71 ± 1.5	8.9 ± 0.5	7 ± 0.5	45.7 ± 1.4	21 ± 0.5
Fe_3O_4@SiO_2/d-TiO_2_20-Pt0.1	5.49 ± 0.05	68 ± 2	9.1 ± 0.6	7 ± 1	47.2 ± 4.0	24 ± 0.5
Fe_3O_4@SiO_2/d-TiO_2_20-Cu0.1	7.81 ± 0.17	57 ± 2	13.3 ± 1.4	5 ± 1	37.1 ± 1.8	28 ± 1.5
Fe_3O_4@SiO_2/d-TiO_2_20-Pt0.1/Cu0.1	5.48 ± 0.05	69 ± 1	7.9 ± 0.4	8 ± 0.5	42.6 ± 3.3	22 ± 1

MOST WIEDZY Downloaded from mostwiedzy.pl

The XRD analysis of Fe_3O_4@SiO_2/d-TiO_2-Pt/Cu confirmed the formation of a magnetic composite, and, as observed in Figure 3 and Table 4, there was no significant difference between the diffraction patterns of the obtained magnetic photocatalysts modified with Pt/Cu NPs. The presence of pure magnetite, with diffraction peaks at 30.2°, 35.6°, 43.3°, 57.3°, and 62.9° 2θ corresponding to (220), (311), (400), (511), and (440) cubic inverse spinel planes (ICDD's card No. 9005813) was confirmed for all Fe_3O_4@SiO_2/d-TiO_2-Pt/Cu magnetic photocatalysts. The decrease in Fe_3O_4 peaks intensity was caused by the formation of tight non-magnetic shell on the core surface, which was previously described by Zielińska-Jurek et al. [26]. The broad peak at 15–25° 2θ corresponds to amorphous silica [38,39]. The content of the magnetite crystalline phase varied from 21% to 28% for Fe_3O_4@SiO_2/d-TiO_2_20-Pt0.05 and Fe_3O_4@SiO_2/d-TiO_2_20-Cu0.1, respectively. At the same time, TiO_2 crystallite size and anatase to rutile phase content ratio remained unchanged for Fe_3O_4@SiO_2/d-TiO_2_20 and Fe_3O_4@SiO_2/d-TiO_2_20-Pt/Cu samples. No other crystalline phases were identified in the XRD patterns, which indicated the crystal purity of the obtained composites.

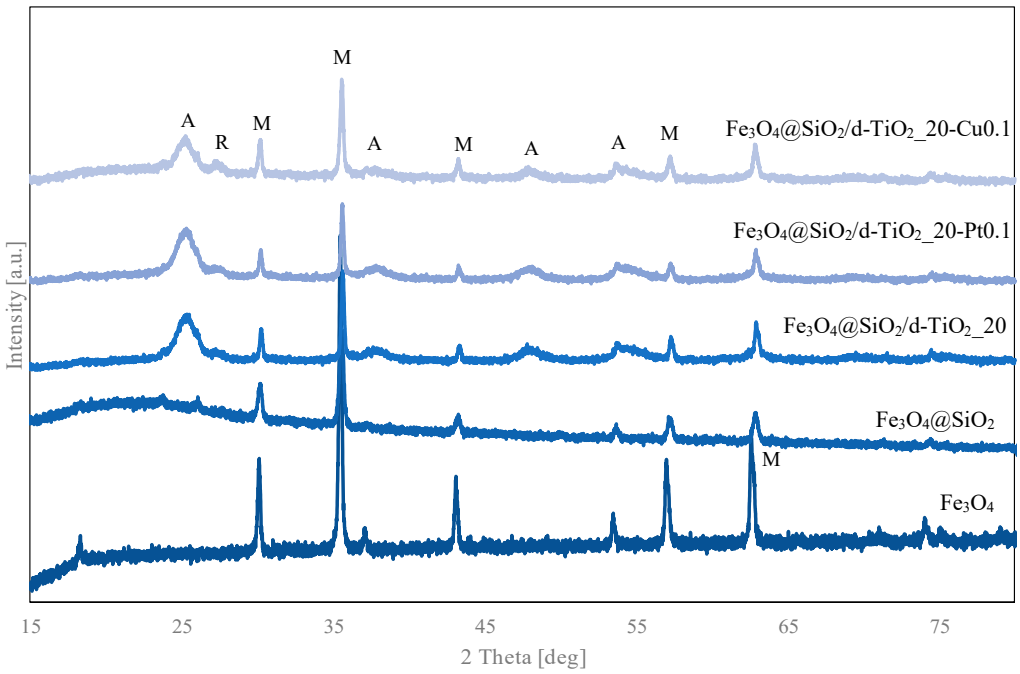

Figure 3. XRD patterns of magnetic photocatalysts, compared with Fe_3O_4 and Fe_3O_4@SiO_2 (A—anatase, R—rutile, and M—magnetite).

The photoabsorption properties of metal-modified defective d-TiO_2 samples were studied by diffuse reflectance spectroscopy, and exemplary data are shown in Figure 4. Comparing to pure TiO_2 photocatalyst, introducing platinum as a surface modifier caused an increase of absorption in the visible light region, however, without shifting a maximum, as presented for sample TiO_2–Pt0.05. Modification of defective d-TiO_2 with Pt and Cu was associated with a further increase of Vis light absorbance and proportional to the amount of the deposited metal. Moreover, the deposition of Pt caused a more significant absorbance increment than the same modification with Cu species.

MOST WIEDZY Downloaded from mostwiedzy.pl

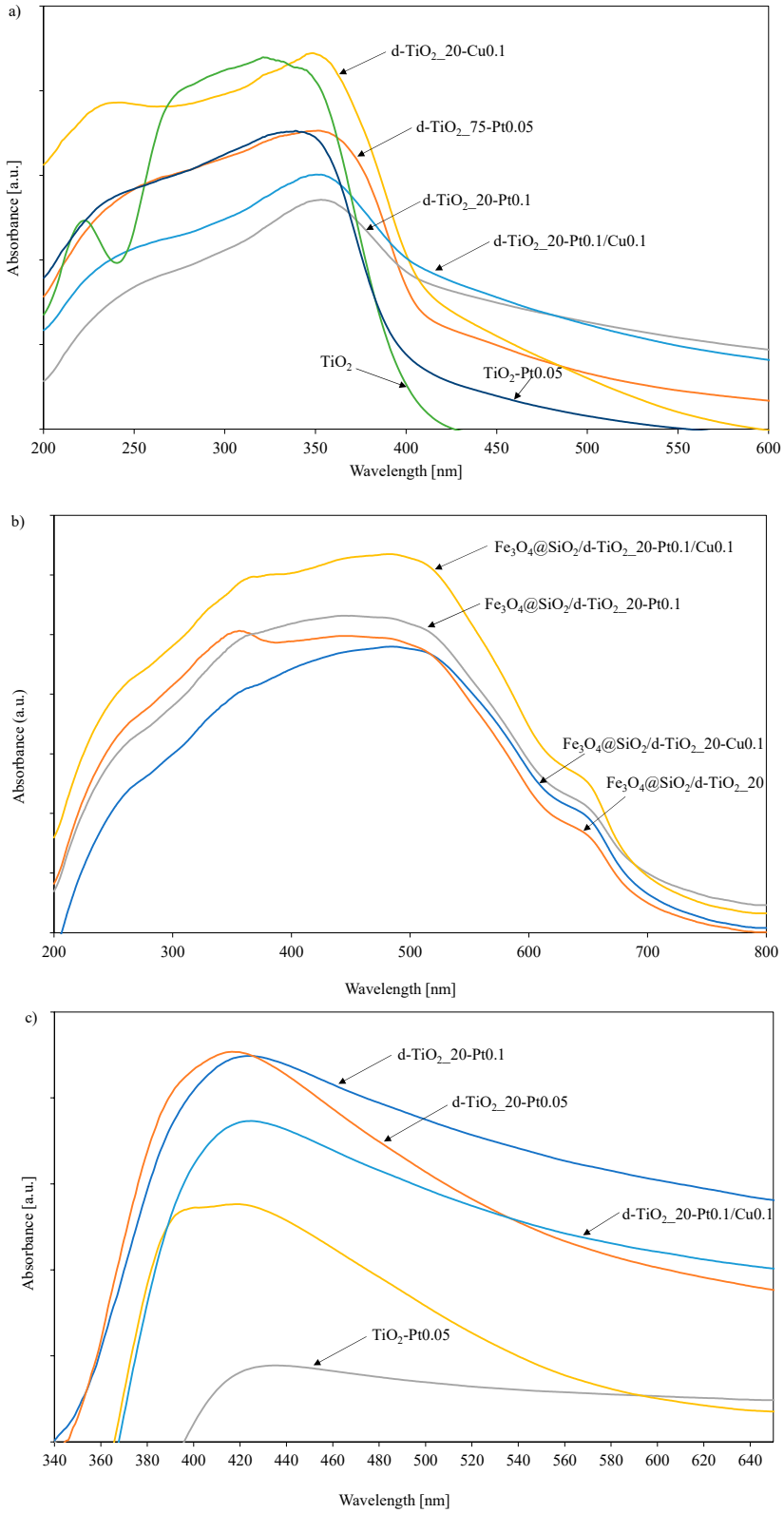

Figure 4. DR/UV-Vis spectra for selected d-TiO_2-Pt/Cu (**a**) and Fe_3O_4@SiO_2/d-TiO2-Pt/Cu (**b**) photocatalysts together with Pt and Cu plasmon determination with bare TiO_2 as a reference (**c**).

Defective d-TiO_2-Pt/Cu deposited on Fe_3O_4@SiO_2 core were characterized by extended light absorption ranged to 700 nm. It could be observed that the described absorption properties in the Vis light for metal-modified TiO_2 and absorption properties of final composites have been preserved.

MOST WIEDZY Downloaded from mostwiedzy.pl

The presence of Localized Surface Plasmon Resonance (LSPR) peaks for Pt and Cu were confirmed based on DR-UV/Vis spectra measurements with pure TiO_2 as a reference (see in Figure 4c). Platinum surface plasmon resonance was observed at the wavelength of about 410–420 nm [33,40]. Electron transfer between Cu(II) and valence band of titanium(IV) oxide could be confirmed by absorption increment from 400 to 450 nm. The typical LSPR signal for zero valent copper at 500–580 nm was not observed, suggesting that Cu is mainly present in its oxidized forms [41,42].

To confirm the presence of noble metal and semi-noble metal NPs on defective TiO_2 surface, the XPS analyses for the selected photocatalysts and deconvolution of Pt 4f and Cu 2p were performed, and the results are presented in Figure 5. Platinum species deposited on the titania surface were designated by deconvolution of Pt 4f peak into two components: Pt $4f_{7/2}$ and Pt $4f_{5/2}$. According to the literature, Pt $4f_{7/2}$ peak, with binding energies in the range of 74.2 to 75.0 eV, refers to the Pt^0, while Pt $4f_{5/2}$ peak, appearing at 77.5–77.9 eV is assigned to Pt^{4+} [11]. The main peaks for Cu 2p appeared as Cu $2p_{3/2}$ and Cu $2p_{1/2}$ at 934 eV and 952 eV. Both of those peaks are commonly attributed to Cu^+ and Cu^{2+} ions [13,43,44]. Obtained data indicated that both Pt and Cu species were successfully deposited on the titania surface.

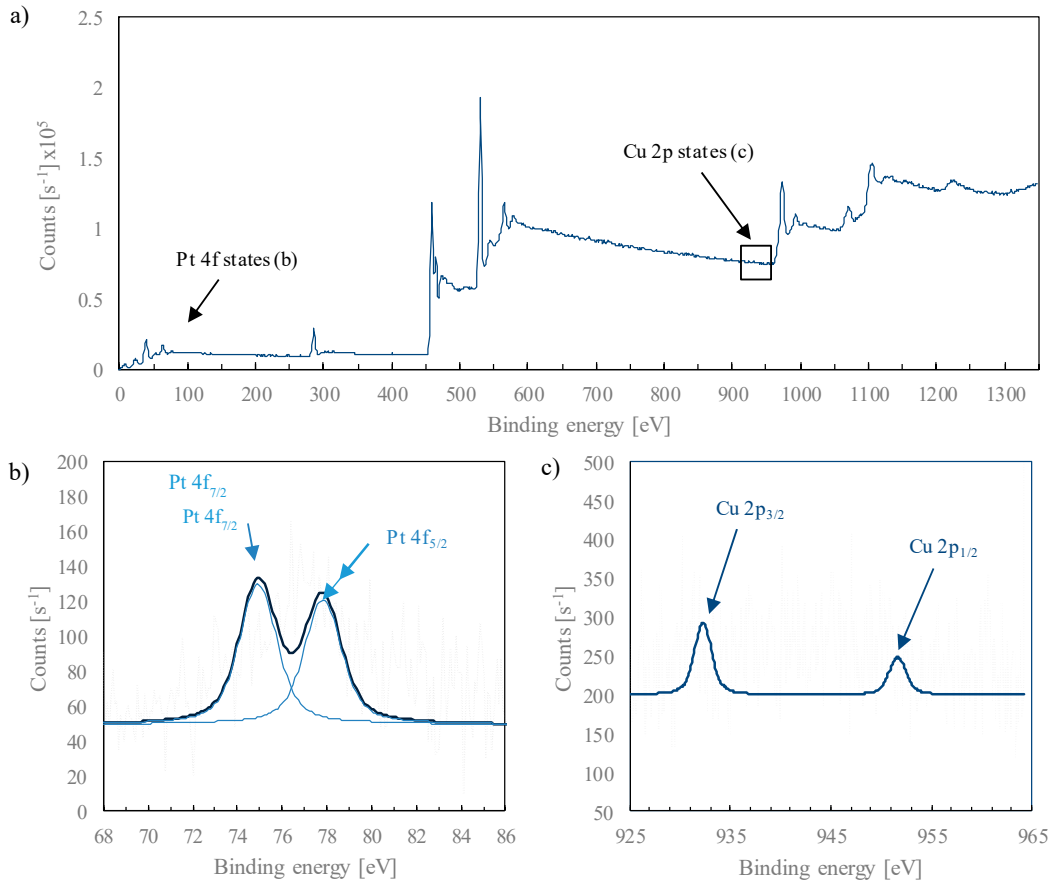

Figure 5. XPS spectra for d-TiO_2_20-Pt0.1/Cu0.1 sample (**a**) with the deconvolution for Pt 4f (**b**) and Cu 2p (**c**).

Moreover, the presence of Pt NPs at the surface of the magnetic nanocomposites was also confirmed by microscopy analysis. As presented in Figure 6, the formation of SiO_2/TiO_2 shell, with a thickness of about 20 nm, tightly covering magnetite nanoparticles was observed. Platinum nanoparticles with a diameter of about 10–20 nm were evenly distributed on the d-TiO_2 layer.

MOST WIEDZY Downloaded from mostwiedzy.pl

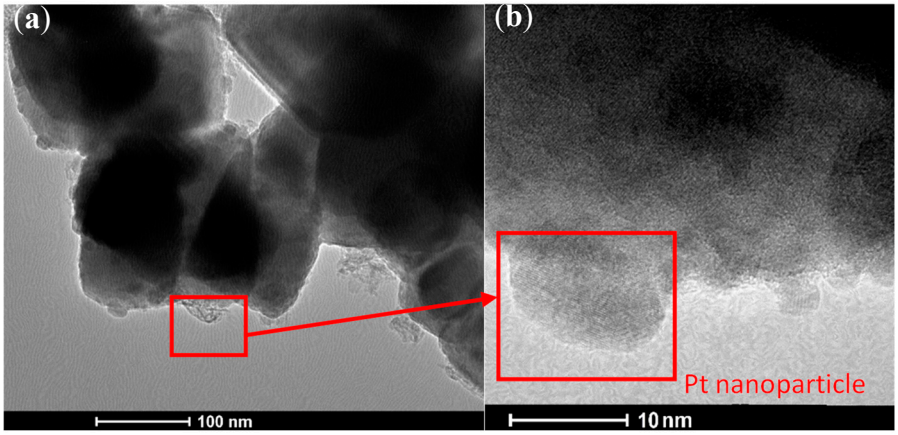

Figure 6. Transmission electron microscopy (TEM) analysis for Fe_3O_4@SiO_2/d-TiO_2_20/Pt0.1 sample (**a**) magnification on Pt nanoparticle (**b**).

2.2. Photocatalytic Activity of d-TiO_2-Pt/Cu and Fe_3O_4@SiO_2/d-TiO_2-Pt/Cu Photocatalysts

The effect of Pt and Cu presence on the properties of defective d-TiO_2 photocatalysts was evaluated in reaction of phenol degradation under UV-Vis and Vis light irradiation. The results, presented as the efficiency of phenol degradation as well as phenol degradation rate constant k, are given in Figures 7 and 8. Additionally, the effect of the electron (e^-), hole (h^+), hydroxyl radical ($^\bullet OH$), and superoxide radical ($^\bullet O_2^-$) scavengers were investigated and presented in Figure 9.

Among analyzed metal-modified photocatalysts, TiO_2–Pt0.05 revealed the highest phenol degradation in UV-Vis light. After 60 min of irradiation, about 76% of phenol was degraded. After introducing plasmonic platinum and semi-noble copper species as a surface modifiers, UV-Vis photoactivity of defective d-TiO_2 samples increased to 59%. The degradation rate constant k increased to 1.47×10^{-2} min^{-1} compared to d-TiO_2_20 (0.79×10^{-2} min^{-1}), and d-TiO_2_75 (0.52×10^{-2} min^{-1}) photocatalysts. Nonetheless, the most significant changes were observed during the photocatalytic process in visible light ($\lambda > 420$ nm). Modifying with 0.05 mol% of Pt, the surface of almost inactive in Vis light d-TiO_2_75 resulted in three-times higher photocatalytic activity under visible light. Therefore, a highly positive effect of metal surface modification of defective d-TiO_2 photocatalyst surface was noticed. It resulted from better charge carriers' separation and decreasing the electron-hole recombination rate. Moreover, the narrower bandgap of the defective d-TiO_2 (in comparison with pure TiO_2) and modification with Pt possessing surface plasmon resonance properties, could also enhance visible light absorption and consequently led to photocatalytic activity increase.

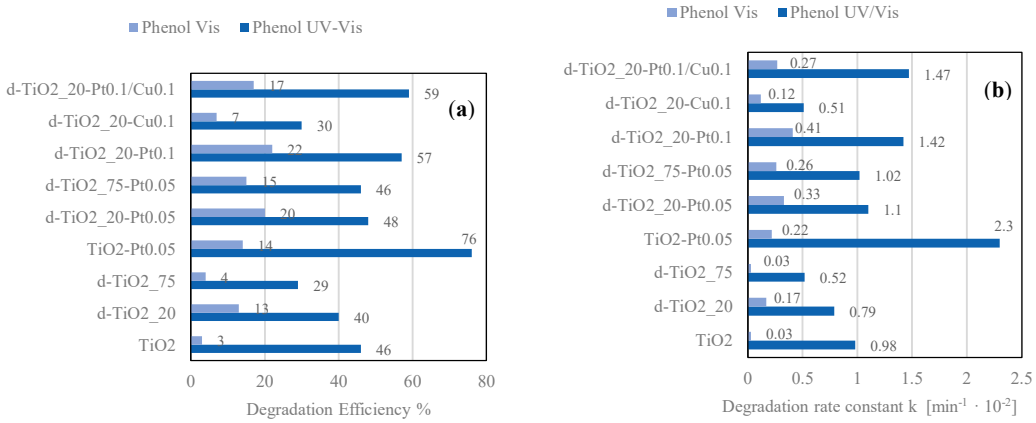

Figure 7. Efficiency of phenol degradation in UV-Vis and Vis light for d-TiO_2-Pt/Cu photocatalysts, presented as % of degradation (**a**) and rate constant k (**b**).

MOST WIEDZY Downloaded from mostwiedzy.pl

Pure magnetite, coated with inert silica, did not affect the photocatalytic process. Furthermore, the Fe_3O_4@SiO_2/d-TiO_2 composite modified with Pt NPs, and bimetallic Pt/Cu NPs revealed the highest photocatalytic activity in Vis light range. The phenol degradation rate constant in Vis light was 2-times higher for Fe_3O_4@SiO_2/d-TiO_2-Pt/Cu compared to Fe_3O_4@SiO_2/d-TiO_2 sample. However, the obtained magnetic photocatalysts had similar photocatalytic activity in UV-Vis light, almost regardless of the surface modification of d-TiO_2 with noble metals. It probably resulted from larger Pt particles (~20 nm) deposition at the surface of Fe_3O_4@SiO_2/d-TiO_2 composite than for TiO_2–Pt0.05 with particles size of about 2–3 nm. Previously, we have reported that the size of noble metal nanoparticles, especially platinum, deposited on the TiO_2 surface strictly depends on the semiconductor surface area, as well as its crystal lattice defects [33,45]. Fine metal particles are produced on the TiO_2 surface with a developed specific surface area with a high density of oxygen traps and nucleation sites, and the highest photocatalytic activity is noticed for Pt-modified photocatalyst, where the size of Pt is below 3 nm [33]. In the present study, Pt nanoparticles' average diameter was about 20 nm as a result of the deposition of Pt ions and their reduction on formed particles' defects. Therefore, the lower metal/semiconductor interface resulted in a decrease in photocatalytic activity under UV-Vis light irradiation.

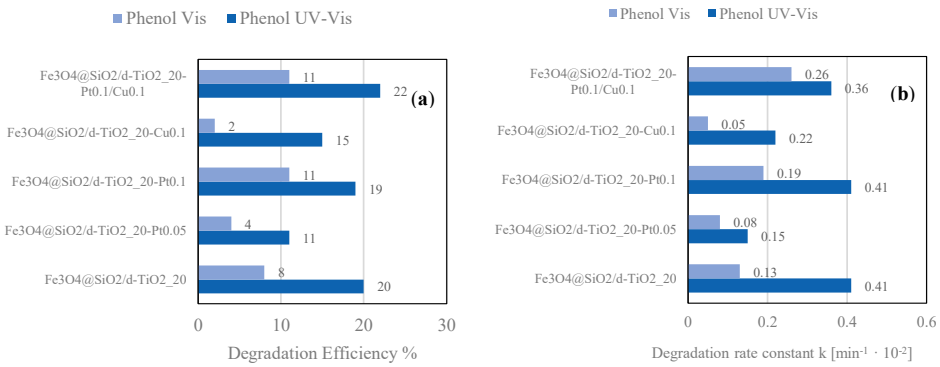

Figure 8. Efficiency of phenol degradation in UV-Vis and Vis light for magnetic Fe_3O_4@SiO_2/d-TiO_2-Pt/Cu photocatalysts, presented as % of degradation (**a**) and rate constant k (**b**).

For the final stability and reusability test, the most active defective photocatalyst was selected. For sample d-TiO_2_20/Pt0.1/Cu0.1, three 1-h-long subsequent cycles of phenol degradation under UV-Vis light were performed. The obtained results are presented in Figure 9.

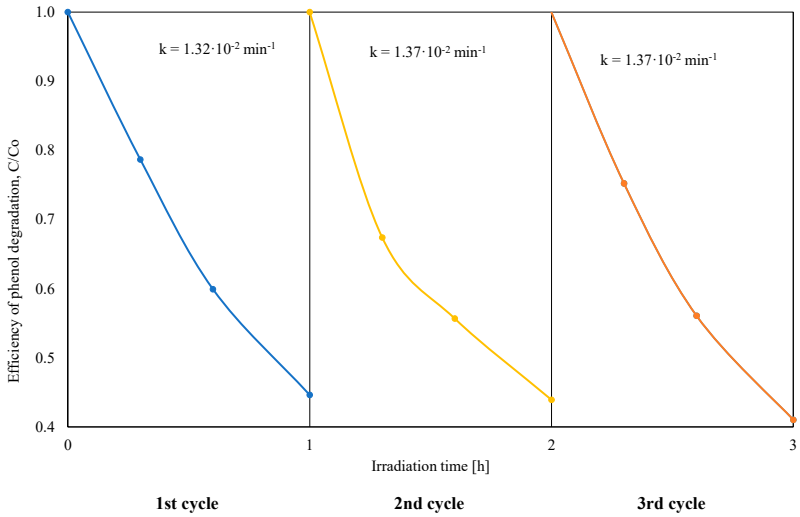

Figure 9. Efficiency of UV-Vis phenol degradation in the presence of defective d-TiO_2_20/Pt0.1/Cu0.1 photocatalyst measured in the three subsequent cycles.

MOST WIEDZY Downloaded from mostwiedzy.pl

There was no significant change in phenol degradation rate constant after the second and third cycles. Thus, the analyzed photocatalyst revealed good stability and reusability.

Furthermore, the reactive species were investigated to understand the photocatalytic reaction mechanism. Benzoquinone (BQ), silver nitrate (SN), ammonium oxalate (AO), and tert-butanol (t-BuOH) were used as superoxide radical anions ($\cdot O_2^-$), electrons (e^-), holes (h^+), and hydroxyl radicals ($\cdot$OH) scavengers, respectively. Obtained results, presented as phenol degradation rate constant k, in comparison to the photodegradation process without scavengers, are presented in Figure 10. The most significant impact on phenol degradation reaction in the presence of metal-modified d-TiO_2 was observed for superoxide radicals. After introducing to the photocatalyst suspension BQ solution, the phenol degradation efficiency was significantly inhibited. A slight decrease was also observed in the presence of SN as an electron trap. On the other hand, the addition of AO and t-BuOH did not decrease the phenol degradation rate.

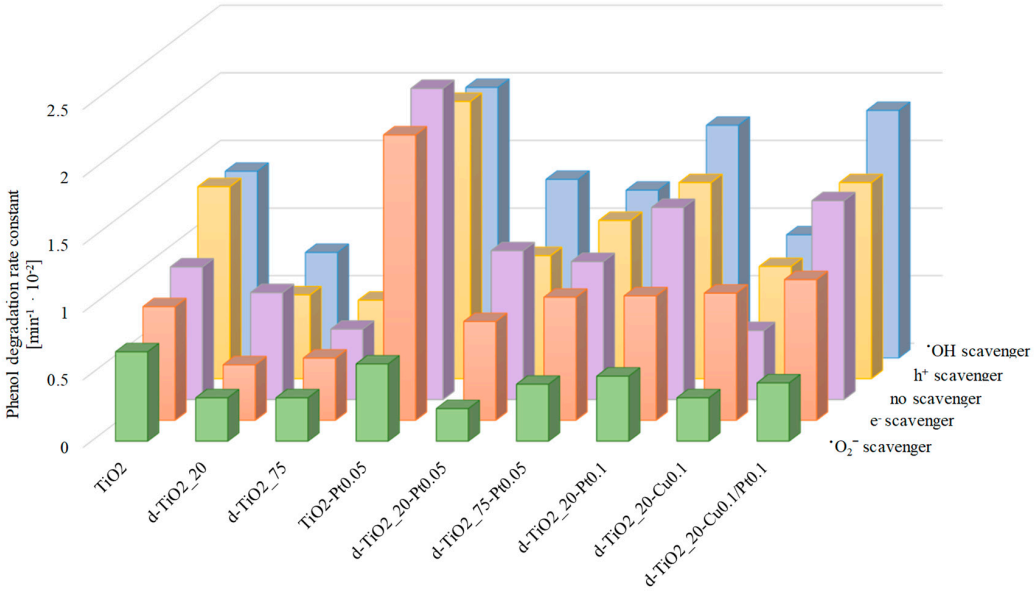

Figure 10. Photocatalytic degradation of phenol for defective Fe_3O_4@SiO_2/d-TiO_2-Pt/Cu photocatalysts in the presence of e^-, h^+, $^{\bullet}O_2^-$, and $^{\bullet}$OH scavengers.

Modification of TiO_2 resulted in the shift of the valence band as was revealed from the analysis of Mott–Schottky plot, where the relation between applied potential vs. Csc^{-2} is presented (see in Figure 11). According to the intersection with E axis the flat band potential was estimated. In the case of pure titania it equals to −1.2 V, whereas for d-TiO_2_20-Pt0 the value of −1.13 was reached. In order to prepare energy diagram of both materials given in Figure 12, the values of bandgap energy was taken into account. As could be seen, for the modified material the position both the conduction and valence band are shifted. According to Monga et al. [46] the Schottky barrier formed at the metal-TiO_2 interface affecting the efficiency of e- transfer. The lowering of the CB band edge is in accordance with the literature indicating that the work function of the metal prone decrease of the CB location. Then, the Schotky barrier is decreased at the metal/semiconductor heterojunction. As a result, the transfer of the photoexcited electron from metal NPs to titania is facilitated and plays important role in photocatalytic activity improvement. The introduction of titanium defects to the TiO_2 crystal structure also resulted in narrowing the bandgap from 3.2 to 2.7 eV.

Based on the presented results, a schematic mechanism of UV-Vis phenol degradation in the presence of metal-modified defective Fe_3O_4@SiO_2/d-TiO_2-Pt/Cu photocatalyst was proposed and shown in Figure 12. After irradiation of the photocatalyst surface with UV-Vis light, electrons from the Pt are injected to the conduction band of titania and then utilized in oxygen reduction to form

MOST WIEDZY Downloaded from mostwiedzy.pl

reactive oxygen radicals. The path of phenol degradation led through several intermediates, such as benzoquinone, hydroquinone, catechol, resorcinol, oxalic acid, and finally, to complete mineralization to CO_2 and H_2O [47–49]. An analysis of possible charge carriers' impact revealed that for photoactivity of d-TiO_2-Pt/Cu, they are responsible for mainly generated superoxide radicals. The phenol degradation mechanism proceeded by the generation of reactive oxygen species, e.g., $^{\bullet}O_2^-$, which attacked the phenol ring, resulting in benzoquinone and hydroquinone formation confirmed by high-performance liquid chromatography (HPLC) analyses. Moreover, during the photoreaction, the concentration of formed intermediates decreased, which suggests mineralization of recalcitrant chemicals to simple organic compounds.

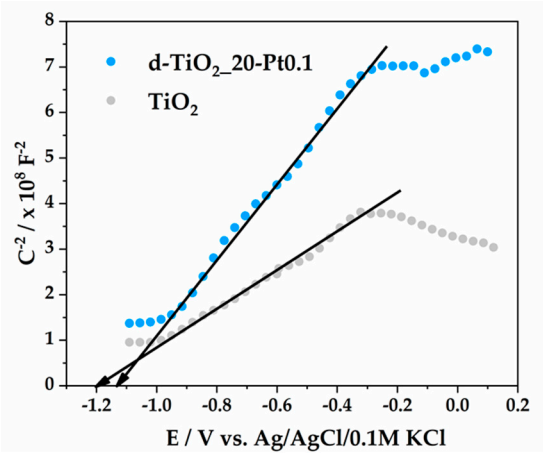

Figure 11. The Mott–Schottky plot for the bare and Pt modified d-TiO_2.

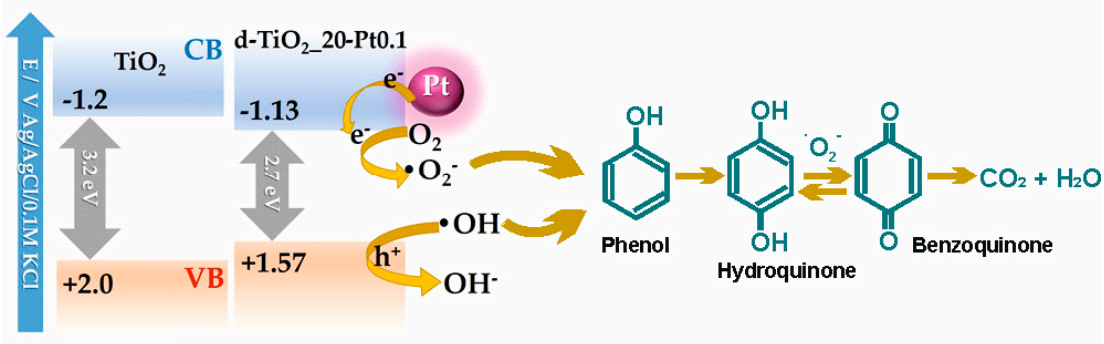

Figure 12. Energy diagram depicting the position of valence and conduction bands of bare and modified titania including the indication of charge transfer within the Schottky junction, and schematic illustration of phenol degradation mechanism over defective Fe_3O_4@SiO_2/d-TiO_2-Pt/Cu photocatalysts.

3. Materials and Methods

Titanium(IV) oxide organic precursor: titanium(IV) butoxide (>99%) was provided by Alfa Aesar (Haverhill, MA, USA). Iodic acid (99.5%), sodium borohydride (99%), chloroplatinate acid hydrate ($H_2PtCl_4 \cdot xH_2O$) (99.9%) and copper nitrate trihydrate ($Cu(NO_3)_2 \cdot 3H_2O$) (99–104%), used for TiO_2 structure and surface modification, were purchased from Sigma (Poznan, Poland). Ferrous ferric oxide (Fe_3O_4, 97%) with a declared particles size of 50 nm was purchased from Aldrich (Poznan, Poland). Tetraethyl orthosilicate (TEOS) was provided by Aldrich and was used as a precursor for the inert interlayer of magnetic nanoparticles. Ammonium hydroxide solution (25%) was purchased from Avantor (Gliwice, Poland). Chemicals for w/o microemulsions preparation, such as cyclohexane and 2-propanol, were purchased from Avantor. Cationic surfactant, hexadecyltrimethylammonium bromide (CTAB), was provided by Sigma Aldrich (Poznan, Poland). Acetonitrile and orthophosphoric acid (85%) for HPLC mobile phase preparation were provided by Merck (Darmstadt, Germany)

MOST WIEDZY Downloaded from mostwiedzy.pl

and VWR (Gdansk, Poland), respectively. Phenol, used as a model organic recalcitrant pollutant in photocatalytic activity measurements, was purchased from VWR. For the titania paste formation polyethylene glycol (PEG) from Sigma Aldrich (Poznan, Poland) was used, while Na_2SO_4 used for electrolyte preparation was purchase from VWR. All reagents were used without further purification.

3.1. Preparation of Defective TiO_2-Pt/Cu Photocatalysts

Defective TiO_2 (marked as d-TiO_2) was obtained by the hydrothermal method assisted with the annealing process. Titanium(IV) butoxide (TBT) and iodic acid (HIO_3) were used as a TiO_2 precursor and oxidizing environment for titanium vacancies formation, respectively. Briefly, the appropriate amount of HIO_3 (presented in Table 5) was dissolved in 80 cm^3 of distilled water. After that, 10 cm^3 of TBT was added dropwise, and the obtained suspension was stirred for 1 h with magnetic stirring at room temperature. In the next step, the suspension was transferred into a Teflon-lined autoclave for thermal treatment at 110 °C for 24 h. The resultant precipitate was centrifuged, dried at 70 °C and then calcined at 300 °C for 3 h.

Table 5. HIO_3 concentrations used for the synthesis of each d-TiO_2 photocatalyst.

Sample	Oxidant Concentration [mol%]	Mass of Added Oxidant [g]
TBT	0	0
d-TiO_2_20	20	1.032
d-TiO_2_75	75	3.869

The obtained defective d-TiO_2 photocatalysts were modified using platinum and copper nanoparticles by the co-precipitation method. In this regard, d-TiO_2 was dispersed in 50 cm^3 of deionized water, and Pt/Cu precursor solutions (0.05 and 0.1 mol% of Pt and 0.1 mol% of Cu with respect to TiO_2) were added. After that, $NaBH_4$ solution was introduced to reduce the metals ions followed by their deposition on the titania surface. The mole ratio of metal ions to $NaBH_4$ was 1:3. After the reduction process, the photocatalyst suspension was mixed for 2 h, and the d-TiO_2-Pt/Cu nanoparticles were separated, washed with deionized water, and dried at 80 °C to dry mass. The final step was calcination at 300 °C for 3 h.

3.2. Preparation of Magnetic Fe_3O_4@SiO_2/d-TiO_2-Pt/Cu Nanocomposites

Previously obtained d-TiO_2-Pt/Cu nanoparticles were deposited on a magnetic substrate as a thin photocatalytic active shell. Magnetite (Fe_3O_4) was selected as a core of the designed composite due to its excellent magnetic properties (high Ms value and low Hc), which enable us to separate obtained photocatalyst in the external magnetic field. Silica was used as an interlayer to isolate Fe_3O_4 from TiO_2 and suppress possible electron transfer between them. The magnetic photocatalysts were obtained in the w/o microemulsion system based on changes in the particles surface charge as a function of pH, described in the previous study [26].

Firstly, commercially available Fe_3O_4 nanoparticles with nominate particles diameter of 50 nm were dispersed in water at pH 10. The prepared suspension was then introduced to cyclohexane/isopropanol (100:6 volume ratio) mixture in the presence of cationic surfactant and cetyltrimethylammonium bromide (CTAB) creating stable w/o microemulsion system with water nanodroplets dispersed in the continuous oil phase. The molar ratio of water to surfactant was set at 30. After the microemulsion stabilization, the corresponding amount of tetraethyl orthosilicate (TEOS) was added, resulting in the formation of SiO_2 interlayer on Fe_3O_4 core, after ammonia solution introduced into the microemulsion system. The molar ratio of TEOS to Fe_3O_4 was 8:1, and NH_4OH to TEOS was 16:1. The microemulsion was destabilized using acetone and obtained nanocomposite Fe_3O_4@SiO_2 was separated, washed with ethanol and water, dried at 70 °C to dry mass, and calcined at 400 °C for 2 h.

In the second step, previously obtained Fe_3O_4@SiO_2 particles were combined with d-TiO_2-Pt/Cu in order to create photocatalytic active nanomaterial. The reversed-phased microemulsion system at

MOST WIEDZY Downloaded from mostwiedzy.pl

pH 10 was used, and Fe_3O_4 to the TiO_2 molar ratio was equaled to 1:4 [27]. The junction between magnetic/SiO_2 and photocatalytic layers was promoted by their opposite surface charges, provided by the presence of CTAB at the basic conditions. The as-obtained Fe_3O_4@SiO_2/d-TiO_2-Pt/Cu samples, after their separation and purification using water and ethanol, were dried at 70 °C to dry mass and calcined at 300 °C for 2 h.

3.3. Characterization of the Obtained Magnetic Photocatalysts

The XRD analyses were performed using the Rigaku Intelligent X-ray diffraction system SmartLab equipped with a sealed tube X-ray generator (a copper target; operated at 40 kV and 30 mA). Data was collected in the 2θ range of 5–80° with a scan speed and scan step of 1°·min^{-1} and 0.01°, respectively. The analyses were based on the International Centre for Diffraction Data (ICDD) databased. The crystallite size of the photocatalysts in the vertical direction to the corresponding lattice plane was determined using Scherrer's equation with Scherrer's constant equal to 0.891. Quantitative analysis, including phase composition with standard deviation, was calculated using the Reference Intensity Ratio (RIR) method from the most intensive independent peak of each phase.

Nitrogen adsorption-desorption isotherms (BET method for the specific surface area) were recorded using the Micromeritics Gemini V (model 2365) (Norcross, GA, USA) instrument at 77 K (liquid nitrogen temperature).

Light absorption properties were measured using diffuse reflectance (DR) spectroscopy in the range of 200–800 nm. The bandgap energy of obtained samples was calculated from $(F(R)\cdot E)^{0.5}$ against E graph, where E is photon energy, and F(R) is Kubelka–Munk function, proportional to the radiation's absorption. The measurements were carried out using ThermoScientific Evolution 220 Spectrophotometer (Waltham, MA, USA) equipped with a PIN-757 integrating sphere. As a reference, $BaSO_4$ was used.

X-ray photoelectron spectroscopy (XPS) measurements were conducted using Escalab 250Xi multi-spectrometer (Thermofisher Scientific) using Mg K X-rays.

The morphology and distribution size for Fe_3O_4@SiO_2/d-TiO_2-Pt as a reference magnetic nanocomposite sample was further analyzed using HR-TEM imagining (Tecnai F20 X-Twin, FEI Europe) together with elements identification in nanometric scale by EDS mapping.

Electron paramagnetic resonance (EPR) spectroscopy was used for intrinsic defects formation confirmation. Measurements were conducted using RADIOPAN SE/X-2547 spectrometer (Poznań, Poland), operating at room temperature, with frequency in range 8.910984–8.917817 GHz.

3.4. Photocatalytic Activity Analysis

Photocatalytic activity of the obtained samples was evaluated in phenol degradation reaction, both in UV-Vis and Vis light irradiation, using 300 W Xenon lamp (LOT Oriel, Darmstadt, Germany). For the visible light measurements, a cut-off 420 nm filter (Optel, Opole, Poland) was used to obtain a settled irradiation interval. A 0.05 g (2 g·dm^{-3}) of a photocatalyst, together with a 20 mg·dm^{-3} phenol solution, was added to a 25 cm^3 quartz photoreactor with an exposure layer thickness of 3 cm and obtained suspension was stirred in darkness for 30 min to provide adsorption-desorption equilibrium. After that, photocatalyst suspension was irradiated under continuous stirring and a power flux (irradiation intensity) of 30 mW·cm^{-2} for 60 min. The constant temperature of the aqueous phase was kept at 20 °C using a water bath. Every 20 min of irradiation, 1.0 cm^3 of suspension was collected and filtered through syringe filters (pore size = 0.2 μm) for the removal of photocatalysts particles. Phenol concentration, as well as a formation of degradation intermediates, were analyzed using reversed-phase high-performance liquid chromatography (HPLC) system, equipped with C18 chromatography column with bound residual silane groups (Phenomenex, model 00F-4435-E0) and a UV-Vis detector with a DAD photodiodes array (model SPD-M20A, Shimadzu). The tests were carried out at 45 °C and under isocratic flow conditions of 0.3 mL·min^{-1} and volume composition of the mobile phase of 70% acetonitrile, 29.5% water and 0.5% orthophosphoric acid. Qualitative and

MOST WIEDZY Downloaded from mostwiedzy.pl

quantitative analysis was performed based on previously made measurements of relevant substance standards and using the method of an external calibration curve.

Phenol removal percentage was calculated from the equation:

$$D\% = \frac{C_o - C_n}{C_o} \cdot 100 \quad (1)$$

where: C_o—phenol initial concentration [mg·dm^{-3}], C_n—phenol concentration during photodegradation [mg·dm^{-3}].

Rate constant k was determined from ln(C_o/C_n) against t plot where C_o and C_n are phenol concentrations [mg·dm^{-3}] and t is degradation time [min]. Rate constant k is equal to directional coefficient "a" of the plot.

In order to evaluate the stability of the obtained photocatalysts, three 1-h-long subsequent cycles of phenol degradation under UV-Vis light using the most active defective d-TiO_2_20/Pt0.1/Cu0.1 sample were performed. After each cycle, photocatalyst was separated from the suspension and use in the next cycle without additional treatment.

The effect of charge carrier scavengers was examined by addition into phenol solution 1 cm^3 of 500 mg·dm^{-3} of tert-butyl alcohol (t-BuOH), benzoquinone (BQ), ammonium oxalate (AO), and silver nitrate (SN), respectively.

3.5. Electrochemical Measurements

In order to prepare Mott–Schottky plot the fabricated titania powders were used to form the paste, deposited using doctor-blade technique onto the Pt support. The paste consist of 0.2 g of photocatalyst in 0.1 g of polyethylene glycol (PEG) and 1 cm^3 of deionized water. Finally the calcination was carried out at 400 °C for 5 h with a heating rate 1 °C·min-^{1} ensuring removal of the organic binder. The fabricated electrode material stayed as working electrode tested in three electrode arrangement where Ag/AgCl/0.1M KCl and Pt mesh were used as reference and counter electrode, respectively. The deaerated 0.5 M Na_2SO_4 was applied as electrolyte. The electrochemical spectroscopy (EIS) impedance data was recorded from the anodic towards cathodic direction. Prior the tests, the investigated samples were not subjected to any preliminary treatment or measurement and their potential was held to reach a steady-state conditions. EIS data were recorded for the single frequency of 1000 Hz in the potential range from +0.1 to −1.2 V vs. Ag/AgCl/0.1 M KCl using a 10 mV amplitude of the AC signal. The capacitance of space charge layer was further calculated from the imaginary part of the measured impedance following the equation [50]:

$$C_{SC} = \frac{-1}{2\pi f Z_{im}} \quad (2)$$

where f stands for the frequency of the AC signal and Z_{im} for the imaginary part of impedance.

4. Conclusions

Surface modification of defective d-TiO_2 photocatalyst with platinum and copper nanoparticles resulted in a significant increase in its photocatalytic activity, both in UV-Vis and Vis range. The EPR analysis confirmed the presence of Ti defects in the structure of TiO_2 samples. The highest activity in Vis light was noticed for d-TiO_2 modified with Pt NPs. It resulted from surface plasmon resonance properties of Pt and narrowing the bandgap of the defective d-TiO_2. Among magnetic photocatalysts, the highest activity in Vis light was observed for Pt-modified and Pt/Cu-modified defective d-TiO_2 deposited on Fe_3O_4@SiO_2 magnetic core. Analysis of phenol degradation mechanism revealed that superoxide radicals are mainly responsible for phenol oxidation and mineralization. However, the photocatalytic activity in reaction of phenol degradation in UV-Vis light in the presence of Pt-modified Fe_3O_4@SiO_2/d-TiO_2 with the Pt particle size of about 20 nm was comparable with

MOST WIEDZY Downloaded from mostwiedzy.pl

the activity of Fe_3O_4@SiO_2/d-TiO_2. It resulted from the deposition of Pt NPs in the place of titanium vacancies, and as a consequence formation of larger metal particles due to the seed-mediated growth mechanism on the TiO_2. In this regard, a lower metal/semiconductor interface resulted in a decrease in photocatalytic activity in the UV-Vis spectrum range. Furthermore, the creation of a core-shell magnetic Fe_3O_4@SiO_2/d-TiO_2-Pt/Cu nanostructures allowed an effective separation of the obtained magnetic photocatalysts.

Author Contributions: Conceptualization, A.Z.-J.; Formal analysis, Z.B., S.D., J.R., K.S., and A.S.; Funding acquisition, A.Z.-J.; Investigation, Z.B.; Methodology, A.Z.-J. and Z.B.; Project administration, A.Z.-J.; Writing—original draft, A.Z.-J. and Z.B.; Writing—review and editing, A.Z.-J. and Z.B. All authors have read and agreed to the published version of the manuscript.

Funding: This research was funded by Polish National Science Centre (Grant No. NCN 2016/23/D/ST5/01021).

Acknowledgments: This research was supported by Polish National Science Centre, grant no. NCN 2016/23/D/ST5/01021.

Conflicts of Interest: The authors declare no conflict of interest.

References

1. Al-Mamun, M.R.; Kader, S.; Islam, M.S.; Khan, M.Z.H. Photocatalytic activity improvement and application of UV-TiO_2 photocatalysis in textile wastewater treatment: A review. *J. Environ. Chem. Eng.* **2019**, *7*, 103248. [CrossRef]
2. Zhu, D.; Zhou, Q. Action and mechanism of semiconductor photocatalysis on degradation of organic pollutants in water treatment: A review. *Environ. Nanotechnol. Monit. Manag.* **2019**, *12*, 100255. [CrossRef]
3. Ahmad, K.; Ghatak, H.R.; Ahuja, S.M. Photocatalytic Technology: A review of environmental protection and renewable energy application for sustainable development. *Environ. Technol. Innov.* **2020**, *19*, 100893. [CrossRef]
4. Wang, K.; Janczarek, M.; Wei, Z.; Raja-Mogan, T.; Endo-Kimura, M.; Khedr, T.M.; Ohtani, B.; Kowalska, E. Morphology- and Crystalline Composition-Governed Activity of Titania-Based Photocatalysts: Overview and Perspective. *Catalysts* **2019**, *9*, 1054. [CrossRef]
5. Koe, W.S.; Lee, J.W.; Chong, W.C.; Pang, Y.L.; Sim, L.C. An overview of photocatalytic degradation: Photocatalysts, mechanisms, and development of photocatalytic membrane. *Environ. Sci. Pollut. Res.* **2020**, *27*, 2522–2565. [CrossRef] [PubMed]
6. Loeb, S.K.; Alvarez, P.J.J.; Brame, J.A.; Cates, E.L.; Choi, W.; Crittenden, J.; Dionysiou, D.D.; Li, Q.; Li-Puma, G.; Quan, X.; et al. The Technology Horizon for Photocatalytic Water Treatment: Sunrise or Sunset? *Environ. Sci. Technol.* **2019**, *53*, 2937–2947. [CrossRef] [PubMed]
7. Serpone, N. Is the Band Gap of Pristine TiO_2 Narrowed by Anion- and Cation-Doping of Titanium Dioxide in Second-Generation Photocatalysts? *J. Phys. Chem. B* **2006**, *110*, 24287–24293. [CrossRef] [PubMed]
8. Dozzi, M.V.; Selli, E. Doping TiO_2 with p-block elements: Effects on photocatalytic activity. *J. Photochem. Photobiol. C Photochem. Rev.* **2013**, *14*, 13–28. [CrossRef]
9. Diaz-Angulo, J.; Gomez-Bonilla, I.; Jimenez-Tohapanta, C.; Mueses, M.; Pinzon, M.; Machuca-Martinez, F. Visible-light activation of TiO_2 by dye-sensitization for degradation of pharmaceutical compounds. *Photochem. Photobiol. Sci.* **2019**, *18*, 897–904. [CrossRef]
10. Endo-Kimura, M.; Janczarek, M.; Bielan, Z.; Zhang, D.; Wang, K.; Markowska-Szczupak, A.; Kowalska, E. Photocatalytic and Antimicrobial Properties of Ag2O/TiO2 Heterojunction. *ChemEngineering* **2019**, *3*, 3. [CrossRef]
11. Wysocka, I.; Kowalska, E.; Ryl, J.; Nowaczyk, G.; Zielińska-Jurek, A. Morphology, Photocatalytic and Antimicrobial Properties of TiO_2 Modified with Mono- and Bimetallic Copper, Platinum and Silver Nanoparticles. *Nanomaterials* **2019**, *9*, 1129. [CrossRef]
12. Klein, M.; Grabowska, E.; Zaleska, A. Noble metal modified TiO_2 for photocatalytic air purification. *Physicochem. Probl. Miner. Process.* **2015**, *51*, 49–57.
13. Janczarek, M.; Wei, Z.; Endo, M.; Ohtani, B.; Kowalska, E. Silver- and copper-modified decahedral anatase titania particles as visible light-responsive plasmonic photocatalyst. *J. Photonics Energy* **2016**, *7*, 12008. [CrossRef]

MOST WIEDZY Downloaded from mostwiedzy.pl

14. Wei, Z.; Janczarek, M.; Endo, M.; Wang, K.; Balcytis, A.; Nitta, A.; Mendez-Medrano, M.G.; Colbeau-Justin, C.; Juodkazis, S.; Ohtani, B.; et al. Noble Metal-Modified Faceted Anatase Titania Photocatalysts: Octahedron versus Decahedron. *Appl. Catal. B Environ.* **2018**, *237*, 574–587. [CrossRef] [PubMed]
15. Wu, Q.; Huang, F.; Zhao, M.; Xu, J.; Zhou, J.; Wang, Y. Ultra-small yellow defective TiO_2 nanoparticles for co-catalyst free photocatalytic hydrogen production. *Nano Energy* **2016**, *24*, 63–71. [CrossRef]
16. Liriano-Jorge, C.F.; Sohmen, U.; Özkan, A.; Gulyas, H.; Otterpohl, R. TiO_2 Photocatalyst Nanoparticle Separation: Flocculation in Different Matrices and Use of Powdered Activated Carbon as a Precoat in Low-Cost Fabric Filtration. *Adv. Mater. Sci. Eng.* **2014**, *2014*, 1–12. [CrossRef]
17. Lee, S.-A.; Choo, K.-H.; Lee, C.-H.; Lee, H.-I.; Hyeon, T.; Choi, W.; Kwon, H.-H. Use of Ultrafiltration Membranes for the Separation of TiO_2 Photocatalysts in Drinking Water Treatment. *Ind. Eng. Chem. Res.* **2001**, *40*, 1712–1719. [CrossRef]
18. Ray, S.; Lalman, J.A. Fabrication and characterization of an immobilized titanium dioxide (TiO_2) nanofiber photocatalyst. *Mater. Today Proc.* **2016**, *3*, 1582–1591. [CrossRef]
19. Zielińska-Jurek, A.; Klein, M.; Hupka, J. Enhanced visible light photocatalytic activity of Pt/I-TiO2in a slurry system and supported on glass packing. *Sep. Purif. Technol.* **2017**, *189*, 246–252. [CrossRef]
20. Wei, J.H.; Leng, C.J.; Zhang, X.Z.; Li, W.H.; Liu, Z.Y.; Shi, J. Synthesis and magnetorheological effect of Fe_3O_4-TiO_2 nanocomposite. *J. Phys. Conf. Ser.* **2009**, *149*, 25–29. [CrossRef]
21. Zhang, L.; Wu, Z.; Chen, L.; Zhang, L.; Li, X.; Xu, H.; Wang, H.; Zhu, G. Preparation of magnetic Fe_3O_4/TiO_2/Ag composite microspheres with enhanced photocatalytic activity. *Solid State Sci.* **2016**, *52*, 42–48. [CrossRef]
22. Abbas, M.; Rao, B.P.; Reddy, V.; Kim, C. Fe_3O_4/TiO_2 core/shell nanocubes: Single-batch surfactantless synthesis, characterization and efficient catalysts for methylene blue degradation. *Ceram. Int.* **2014**, *40*, 11177–11186. [CrossRef]
23. Sathishkumar, P.; Viswanathan, R.V.; Anandan, S.; Ashokkumar, M. $CoFe_2O_4/TiO_2$ nanocatalysts for the photocatalytic degradation of Reactive Red 120 in aqueous solutions in the presence and absence of electron acceptors. *Chem. Eng. J.* **2013**, *220*, 302–310. [CrossRef]
24. Jia, Y.; Liu, J.; Cha, S.; Choi, S.; Chang, Y.C.; Liu, C. Magnetically separable Au-TiO_2/nanocube $ZnFe_2O_4$ composite for chlortetracycline removal in wastewater under visible light. *J. Ind. Eng. Chem.* **2017**, *47*, 303–314. [CrossRef]
25. Fu, W.; Yang, H.; Li, M.; Chang, L.; Yu, Q.; Xu, J.; Zou, G. Preparation and photocatalytic characteristics of core-shell structure $TiO_2/BaFe_{12}O_{19}$ nanoparticles. *Mater. Lett.* **2006**, *60*, 2723–2727. [CrossRef]
26. Zielińska-Jurek, A.; Bielan, Z.; Dudziak, S.; Wolak, I.; Sobczak, Z.; Klimczuk, T.; Nowaczyk, G.; Hupka, J. Design and Application of Magnetic Photocatalysts for Water Treatment. The Effect of Particle Charge on Surface Functionality. *Catalysts* **2017**, *7*, 360. [CrossRef]
27. Zielińska-Jurek, A.; Bielan, Z.; Wysocka, I.; Strychalska, J.; Janczarek, M.; Klimczuk, T. Magnetic semiconductor photocatalysts for the degradation of recalcitrant chemicals from flow back water. *J. Environ. Manage.* **2017**, *195*, 157–165. [CrossRef]
28. Wysocka, I.; Kowalska, E.; Trzciński, K.; Łapiński, M.; Nowaczyk, G.; Zielińska-Jurek, A. UV-Vis-Induced Degradation of Phenol over Magnetic Photocatalysts Modified with Pt, Pd, Cu and Au Nanoparticles. *Nanomaterials* **2018**, *8*, 28. [CrossRef]
29. Mrotek, E.; Dudziak, S.; Malinowska, I.; Pelczarski, D.; Ryżyńska, Z.; Zielińska-Jurek, A. Improved degradation of etodolac in the presence of core-shell $ZnFe_2O_4/SiO_2/TiO_2$ magnetic photocatalyst. *Sci. Total Environ.* **2020**, *724*, 138167. [CrossRef]
30. Gad-Allah, T.A.; Fujimura, K.; Kato, S.; Satokawa, S.; Kojima, T. Preparation and characterization of magnetically separable photocatalyst ($TiO_2/SiO_2/Fe_3O_4$): Effect of carbon coating and calcination temperature. *J. Hazard. Mater.* **2008**, *154*, 572–577. [CrossRef]
31. Fan, Y.; Ma, C.; Li, W.; Yin, Y. Synthesis and properties of $Fe_3O_4/SiO_2/TiO_2$ nanocomposites by hydrothermal synthetic method. *Mater. Sci. Semicond. Process.* **2012**, *15*, 582–585. [CrossRef]
32. Shi, F.; Li, Y.; Zhang, Q.; Wang, H. Synthesis of $Fe_3O_4/C/TiO_2$ magnetic photocatalyst via vapor phase hydrolysis. *Int. J. Photoenergy* **2012**, *2012*, 1–8. [CrossRef]
33. Zielińska-Jurek, A.; Wei, Z.; Janczarek, M.; Wysocka, I.; Kowalska, E. Size-Controlled Synthesis of Pt Particles on TiO_2 Surface: Physicochemical Characteristic and Photocatalytic Activity. *Catalysts* **2019**, *9*, 940. [CrossRef]

MOST WIEDZY Downloaded from mostwiedzy.pl

34. Bielan, Z.; Kowalska, E.; Dudziak, S.; Wang, K.; Ohtani, B.; Zielińska-Jurek, A. Mono- and bimetallic (Pt/Cu) titanium(IV) oxide core-shell photocatalysts with UV/Vis light activity and magnetic separability. *Catal. Today* **2020**, in press. [CrossRef]
35. Gamboa, J.A.; Pasquevich, D.M. Effect of Chlorine Atmosphere on the Anatase-Rutile Transformation. *J. Am. Chem. Soc.* **1992**, *75*, 2934–2938. [CrossRef]
36. Byrne, C.; Fagan, R.; Hinder, S.; McCormack, D.E.; Pillai, S.C. New Approach of Modifying the Anatase to Rutile Transition Temperature in TiO_2 Photocatalysts. *RSC Adv.* **2016**, *6*, 95232–95238. [CrossRef]
37. Ricci, P.C.; Carbonaro, C.M.; Stagi, L.; Salis, M.; Casu, A.; Enzo, S.; Delogu, F. Anatase-To-Rutile Phase Transition In Nanoparticles Irradiated By Visible Light. *J. Phys. Chem. C* **2013**, *117*, 785–7857. [CrossRef]
38. Liu, H.; Jia, Z.; Ji, S.; Zheng, Y.; Li, M.; Yang, H. Synthesis of $TiO_2/SiO_2@Fe_3O_4$ magnetic microspheres and their properties of photocatalytic degradation dyestuff. *Catal. Today* **2011**, *175*, 293–298. [CrossRef]
39. Chi, Y.; Yuan, Q.; Li, Y.; Zhao, L.; Li, N.; Li, X.; Yan, W. Magnetically separable $Fe_3O_4@SiO_2@TiO_2$-Ag microspheres with well-designed nanostructure and enhanced photocatalytic activity. *J. Hazard. Mater.* **2013**, *262*, 404–411. [CrossRef] [PubMed]
40. Zielińska-Jurek, A.; Hupka, J. Preparation and characterization of Pt/Pd-modified titanium dioxide nanoparticles for visible light irradiation. *Catal. Today* **2013**, *230*, 181–187. [CrossRef]
41. Bielan, Z.; Kowalska, E.; Dudziak, S.; Wang, K.; Ohtani, B.; Zielinska-Jurek, A. Mono- and bimetallic (Pt/Cu) titanium(IV) oxide photocatalysts. Physicochemical and photocatalytic data for magnetic nanocomposites' shell. *Data Brief* **2020**, *31*, 105814. [CrossRef]
42. Chan, G.H.; Zhao, J.; Hicks, E.M.; Schatz, G.C.; Van Duyne, R.P. Plasmonic Properties of Copper Nanoparticles Fabricated by Nanosphere Lithography. *Nano Lett.* **2007**, *7*, 1947–1952. [CrossRef]
43. Ghodselahi, T.; Vesaghi, M.A.; Shafiekhani, A.; Baghizadeh, A.; Lameii, M. XPS study of the $Cu@Cu_2O$ core-shell nanoparticles. *Appl. Surf. Sci.* **2008**, *225*, 2730–2734. [CrossRef]
44. Li, B.; Luo, X.; Zhu, Y.; Wang, X. Immobilization of Cu(II) in KIT-6 Supported Co3O4 and Catalytic Performance for Epoxidation of Styrene. *Appl. Surf. Sci.* **2015**, *359*, 609–620. [CrossRef]
45. Zielińska-Jurek, A.; Wei, Z.; Wysocka, I.; Szweda, P.; Kowalska, E. The effect of nanoparticles size on photocatalytic and antimicrobial properties of Ag-Pt/TiO_2 photocatalysts. *Appl. Surf. Sci.* **2015**, *353*, 317–325. [CrossRef]
46. Monga, A.; Rather, R.A.; Pal, B. Enhanced co-catalytic effect of Cu-Ag bimetallic core-shell nanocomposites imparted to TiO2 under visible light illumination. *Sol. Energy Mater Sol. Cells* **2017**, *172*, 285–292. [CrossRef]
47. Devi, L.G.; Kavitha, R. A review on plasmonic metal—TiO_2 composite for generation, trapping, storing and dynamic vectorial transfer of photogenerated electrons across the Schottky junction in a photocatalytic system. *Appl. Surf. Sci.* **2016**, *360*, 601–622. [CrossRef]
48. Dang, T.T.T.; Le, S.T.T.; Channei, D.; Khanitchaidecha, W.; Nakaruk, A. Photodegradation mechanisms of phenol in the photocatalytic process. *Res. Chem. Intermed.* **2016**, *42*, 5961–5974. [CrossRef]
49. Esplugas, S.; Gimenez, J.; Contreras, S.; Pascual, E.; Rodriguez, M. Comparison of different advanced oxidation processes for phenol degradation. *Water Res.* **2002**, *36*, 1034–1042. [CrossRef]
50. Beranek, R. (Photo)electrochemical methods for the determination of the band edge positions of TiO_2-based nanomaterials. *Adv. Phys. Chem.* **2011**, *2011*, 80–83. [CrossRef]

© 2020 by the authors. Licensee MDPI, Basel, Switzerland. This article is an open access article distributed under the terms and conditions of the Creative Commons Attribution (CC BY) license (http://creativecommons.org/licenses/by/4.0/).

MOST WIEDZY Downloaded from mostwiedzy.pl